Hybrid plasmon photonic crystal resonance grating for integrated spectrometer biosensor

Hong Guo and Junpeng Guo*

Department of Electrical and Computer Engineering, University of Alabama in Huntsville, Huntsville, Alabama 35899, USA
**Corresponding author: guoj@uah.edu*

Received September 4, 2014; revised December 5, 2014; accepted December 5, 2014;
posted December 8, 2014 (Doc. ID 222490); published January 13, 2015

Using nanofabricated hybrid metal–dielectric nanohole array photonic crystal gratings, a hybrid plasmonic optical resonance spectrometer biosensor is demonstrated. The new spectrometer sensor technique measures plasmonic optical resonance from the first-order diffraction rather than via the traditional method of measuring optical resonance from transmission. The resonance spectra measured with the new spectrometer technique are compared with the spectra measured using a commercial optical spectrometer. It is shown that the new optical resonance spectrometer can be used to measure plasmonic optical resonance that otherwise cannot be measured with a regular optical spectrometer.

OCIS codes: (250.5403) Plasmonics; (300.6190) Spectrometers; (050.1950) Diffraction gratings; (160.5298) Photonic crystals.
http://dx.doi.org/10.1364/OL.40.000249

Guided-mode resonance (GMR) in dielectric grating structures for optical filters and biochemical sensors has been investigated extensively since the early 1990s [1–6]. GMR results from grating-coupled waveguide resonance modes in sub-wavelength grating dielectric structures. Optical interference between the coupled waveguide resonance mode and the transmission/reflection wave gives rise to the optical filter effect in the transmission and reflection regions. In metallic nanostructures, such as periodic nanohole and nanoslit arrays in metal films, the strong resonance effect resulting from the excitation of surface plasmonic-polaritons has also been extensively investigated [7–12]. Traditionally, both GMR and surface plasmonic resonance effects were measured using optical spectrometers. Recently, a new surface plasmonic resonance spectrometer technique was reported: it used super-period metal nanohole and nanoslit gratings [13–16]. The new surface plasmonic resonance spectrometer technique measures surface plasmonic resonance in the first-order diffraction, which is different from traditional surface plasmonic resonance measurements where the resonance spectra and shifts were measured in the zero-order transmission [17,18]. In this work, we first fabricated a photonic crystal resonance grating, and then coated the grating with a thin layer of gold metal film. The thin gold film provides a bonding medium for biomolecules [19]. A low cost CCD imager was used to measure the hybrid plasmonic optical resonance spectrum and the resonance shift due to the bonding of biomolecules in the first-order diffraction. With the metal–dielectric nanohole array grating, a hybrid plasmonic optical resonance spectrometer biochemical sensor has been demonstrated.

Figure 1 illustrates the hybrid metal–dielectric plasmon photonic crystal grating structure. The device is made of a nanohole array grating etched through a gold film and a silicon nitride film deposited on a glass substrate. The diameter of the nanoholes is 240 nm. The silicon nitride film has a thickness of 175 nm. The thickness of the gold film increases from 10 to 20 nm, and then to 50 nm after the time of deposition is increased. The nanoholes are arranged with a small period of 500 nm. For every five columns of nanoholes, one column is removed. Therefore, there is also a large grating period of $P = 2500$ nm. The large grating period P, called the "super-period," provides optical diffraction because it is larger than the wavelength of interest. The super-period P was optimized to have a few diffraction orders so that each has enough optical power, and also to provide a large angular dispersion for measuring the resonance spectra of the devices.

The super-period nanohole grating was fabricated on a transparent Pyrex glass substrate. During fabrication, the glass wafer was first cleaned using the standard procedure. Then, a 175 nm thick silicon nitride layer was deposited onto the glass substrate using a Denton sputter. Next, an e-beam resist layer (ZEP-520A) was spin-coated on top of the silicon nitride layer. The thickness of the e-beam resist layer is about 300 nm. The sample was baked in the oven at 120°C for 30 min. Then, super-period nanoholes were written using an e-beam lithography machine (LEO 1550 SEM) and developed in a ZED-N50 solution at the room temperature. After that, reactive-ion etching (RIE) (Plasma Thermal 790 series) was used to etch through the silicon nitride layer to transfer the nanohole grating pattern to the silicon nitride layer. The plasma pressure for the RIE etching was 100 mTorr. The radio frequency (RF) power was

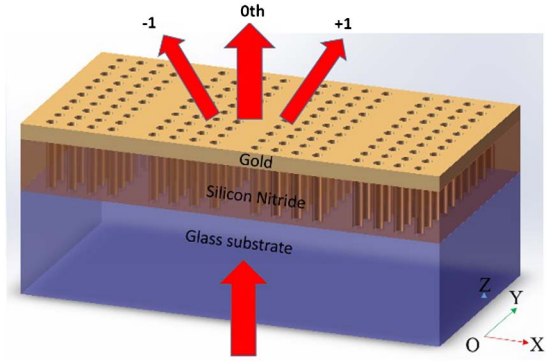

Fig. 1. Schematic of a hybrid plasmon photonic crystal grating.

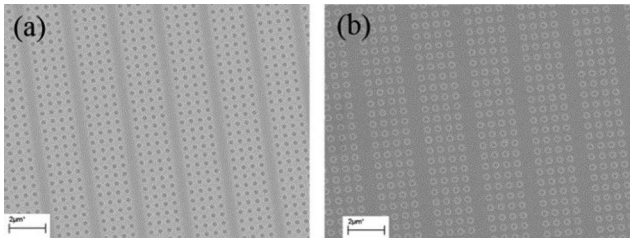

Fig. 2. (a) A SEM image of the super-period nanohole photonic crystal grating. (b) A SEM image of hybrid plasmon photonic crystal grating.

100 W. Oxygen gas flowed at a rate of 4 SCCM and carbon tetrafluoride gas flowed at a rate of 40 SCCM. After the RIE etching, the sample was dipped in the e-beam resist remover solvent (NMP 1165). It remained there at a temperature of 60°C for 2 h to remove the e-beam resist. This was followed by an oxygen-plasma de-scum to remove the e-beam resist residues. The fabricated device was imaged using a scanning electron microscope (SEM). Figure 2(a) shows a SEM image of the fabricated silicon nitride photonic crystal grating with a nanohole diameter of 240 nm and a super-grating period of 2500 nm. The total area of the patterned device area 250 μm × 250 μm.

The zero-order transmission from the fabricated device was first measured using a commercial optical spectrometer (StellarNet C-SR-50) and a broadband light source with a spectral range from 400 to 2400 nm. The incident light comes from the glass substrate with a focused beam diameter of about 185 μm. The transmitted light was collected by an optical fiber collimator and sent to the optical spectrometer. The polarization of the incident light was controlled by a linear polarizer. We set the incident polarization as transverse electric (TE) polarization. The electric field of the TE polarization is parallel to the grating lines in the y direction. The measured transmission spectrum is shown in Fig. 3(a). Two transmission dips are seen in the near infrared region. One occurs at the wavelength of 726 nm and the other is located at the 744.5 nm. The transmission dips are due to the GMR in the two-dimensional photonic crystal.

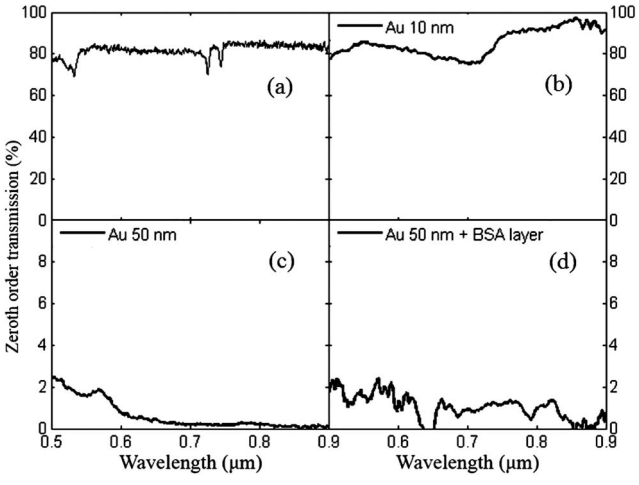

Fig. 3. Zero-order transmission spectra from (a) the super-period nanohole photonic crystal grating, (b) the hybrid plasmon photonic crystal grating with a 10 nm gold layer on the top, (c) the hybrid plasmon photonic crystal grating with a 50 nm gold layer on the top, and (d) the device with a BSA layer bonded on top of the 50 nm gold layer.

After the zero-order transmission was measured, we measured the spectrum of the first-order diffraction. In order to do that, a CCD (Sony ICX098BQ) was placed in one of the first diffraction orders. A helium–neon (HeNe) laser with a wavelength of 632.8 nm was used for calibrating the measurement setup. In the calibration, the distance X between the zero-order transmission spot and the first-order diffraction spot of the HeNe laser on the CCD was first measured [14]. The distance X was used to calculate the distance Z from the device to the CCD with the diffraction angle of the HeNe laser calculated from the wavelength and the super-period P. After X and Z were found, the correspondence between the wavelengths and pixels of the CCD was obtained. The number of pixels of the CCD imager is 640 × 480. The pixel size of the CCD is 5.6 μm × 5.6 μm. The digitized signal for each pixel falls within the range of 0–255. In the measurement, the signal at each diffraction location on the CCD was taken as the sum of all pixel signals in that column. The signals from the CCD were first normalized to the source light spectrum and then normalized to the CCD's responsivity spectrum.

Figure 4(a) shows the first-order diffraction pattern as captured by the CCD. The horizontal and vertical axis labels indicate the location of pixels. The bright spot on the edge on the left side of the CCD image is the diffraction spot from the HeNe laser. In the measurement, we intentionally moved the CCD to let the HeNe laser (632.8 nm wavelength) create a diffraction spot located at the edge of the CCD. Therefore, the data shown in the picture are for the wavelength range from 632.8 nm to longer wavelengths. With the captured first-order diffraction CCD image and the calibration, the spectrum of the first-order diffraction can be obtained. Figure 4(b) shows the resonance spectrum of the dielectric nanohole photonic

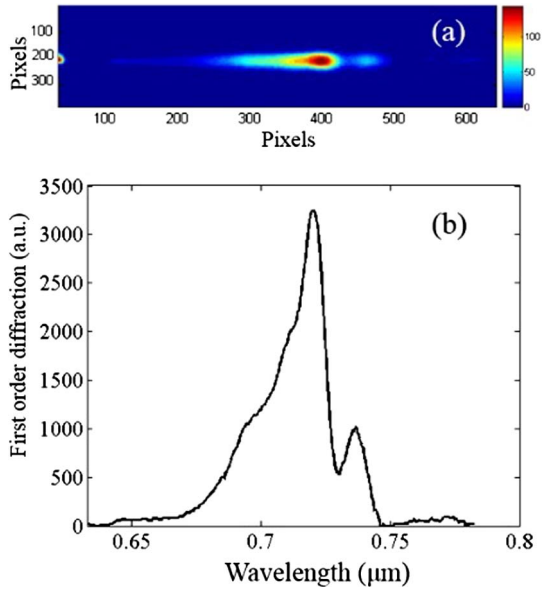

Fig. 4. (a) The first-order diffraction image captured by a CCD. (b) The plot of the optical resonance spectrum obtained from the first-order diffraction CCD image of the dielectric nanohole array photonic crystal grating.

crystal grating obtained from the first-order diffraction. The unit of the first diffraction is the arbitrary unit. It can be seen that two resonance modes at wavelengths of 722.5 and 739.6 nm exist in the device.

After measuring the zero-order transmission and the first-order diffraction from the super-period dielectric photonic crystal grating, we sputtered thin gold films of different thicknesses on the device surface using a Denton sputter. We then repeated the measurements described for the dielectric photonic crystal grating. First, a 10 nm gold layer was sputtered onto the device surface. After measuring the zero-order transmission and the first-order diffraction spectra, an additional 40 nm gold layer was sputtered on the same device, which resulted in a total 50 nm gold layer on the dielectric nanohole grating surface. Figure 2(b) shows a SEM picture of the fabricated hybrid metal–dielectric super-period nanohole grating with a 50 nm gold film on the top. Figure 3(b) shows the zero-order transmission spectrum from the device with a 10 nm gold film sputtered on the top. It can be observed that the optical resonance was broadened and hardly seen after the 10 nm gold film was sputtered on the top. Figure 3(c) shows the zero-order transmission spectrum after an additional 40 nm gold film was sputtered on the device. No optical resonance modes were seen from the zero-order transmission after a total of 50 nm of gold film was sputtered on the device. The zero-order transmittance decreases significantly to 0.55% as a 50 nm gold layer was sputtered due to the conformal coating on the nanohole array surface. Gold was not only deposited on the top of the nanohole grating, but also deposited inside the nanoholes. We measured the first-order diffraction efficiency of the HeNe laser (632.8 nm wavelength) at the normal incidence. The first-order diffraction efficiency is 0.0042%. The ratio of the first-order diffraction over the zero-order transmission is 0.76%. This could indicate that the resonance signal is too small and might be buried in the zero-order transmission. Alternately, it suggests that the gold-coated nanoholes do not radiate efficiently in the direction of the transmission. For the comparison, we also fabricated regular two-dimensional nanohole array devices with the same nanohole size, the same metal–dielectric layer thicknesses, and the same small nanohole period of 500 nm. Since the regular two-dimensional nanohole array devices do not have the super-period P, there is no diffraction. After a 50 nm gold metal layer was deposited on the top, no optical resonance modes were seen in the zero-order transmission spectrum.

The first-order diffraction of the metal–dielectric gratings was measured with same technique for measuring the first-order diffraction of the super-period dielectric nanohole grating. In the experiment, we initially measured the first-order diffraction spectrum for the hybrid metal–dielectric nanohole-grating device with a 10 nm gold layer on the top. We then measured the diffraction spectrum of the device after a 50 nm gold layer was deposited on the top. Figure 5(a) is the first-order diffraction CCD image after a 10 nm gold layer was deposited on the top. Figure 5(b) is the first-order diffraction CCD image after a 50 nm gold layer was deposited on the top.

From the first-order diffraction images captured by the CCD shown in Fig. 5, optical resonance spectra can be

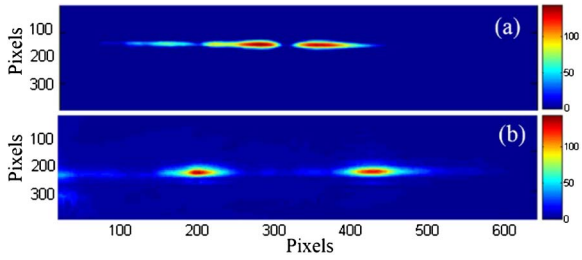

Fig. 5. (a) The first-order diffraction CCD image after a 10 nm gold layer was sputtered onto the dielectric nanohole-grating surface. (b) The first-order diffraction CCD image after a 50 nm gold layer was sputtered onto the device's surface. Each bright spot on the CCD image corresponds to a resonance mode.

obtained with a calibrated wavelength-pixel correspondence. Figure 6(a) shows the optical resonance spectrum measured from the first-order diffraction of the hybrid plasmon photonic crystal grating with a 10 nm gold layer on the top. The first-order diffraction spectrum has an arbitrary unit. There are two resonance modes in the spectrum at wavelengths 754.9 and 695.6 nm. In Fig. 6(b), the solid black line is the optical resonance spectrum obtained from the first-order diffraction of the device with a 50 nm gold layer on the top. One optical resonance mode

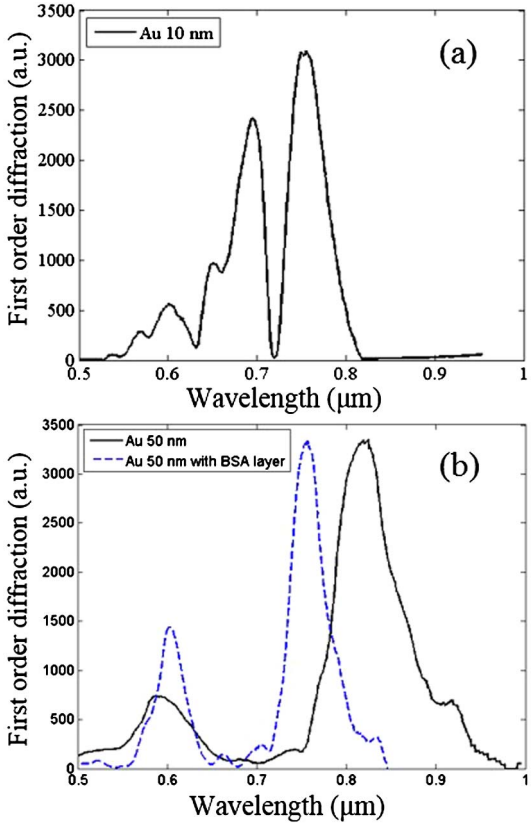

Fig. 6. (a) The optical resonance spectrum measured in the first-order diffraction from the device with a 10 nm gold layer on the top. (b) The solid black line is the optical resonance spectrum obtained from the first-order diffraction of the device with a 50 nm gold layer on the top. The blue dashed line is the optical resonance spectrum obtained from the first-order diffraction for the same device after a BSA protein layer was applied to the device's surface.

is at the wavelength of 824.4 nm. The other optical resonance mode is at the wavelength of 590.5 nm.

After the device with the 50 nm gold layer was measured, a bovine serum albumin (BSA) in a water solution with a concentration of 80 μg/mL was applied to the surface for a biochemical sensor demonstration. BSA is a serum albumin protein derived from cows. It is often used as a protein concentration standard in biochemical lab experiments; in fact, it is one of the most common proteins used in these types of experiments. The measurement was obtained after the water in the BSA solution had completely evaporated. After the water evaporated, an approximately 16 nm thick layer of BSA was left on the device's surface. We first measured the zero-order transmission with a commercial optical spectrometer. The measured zero-order transmission spectrum is shown in Fig. 3(d). It can be seen that no optical resonance mode was found in the zero-order transmission spectrum. Then, we measured the optical resonance of the device with the BSA layer from the first-order diffraction. We also measured the first-order diffraction efficiency from the device without the BSA layer. The optical resonance spectrum measured from the first-order diffraction is shown in the Fig. 6(b) as the blue dashed line curve. It can be seen that after a BSA layer was applied to the surface, the optical resonance wavelengths measured from the first-order diffraction were shifted. The optical resonance wavelength on the red side shifts from 824.4 nm in the air to 755.5 nm after the BSA layer is applied. The total shift is 68.9 nm. The resonance wavelength on the blue side shifts slightly from 602.4 to 590.5 nm. The sensitivity of the surface plasmonic resonance sensors for the biochemical layer bonding was previously defined as the ratio of resonance wavelength shift $\Delta\lambda$ over the thickness Δd of the bonding layer on the surface [18]. To include the effect of the index of refraction of the biochemical bonding layer, we define the sensitivity S_d of our biochemical sensor as

$$S_d = \frac{\Delta\lambda}{\Delta d \times (n_s - n_o)}, \tag{1}$$

where n_s is the refractive index of bonding layer and n_o is the refractive index of the surrounding, which here is air. The refractive index of the BSA layer is 1.572 at the wavelength of 632 nm [20]. The sensitivity of our demonstrated biochemical sensor is 7.53 per refractive index unit.

In summary, we fabricated a super-period photonic crystal nanohole array diffraction grating in a silicon nitride film on a glass substrate. The optical resonance of the super-period photonic crystal grating was measured from the zero-order transmission with an optical spectrometer and then measured from the first-order diffraction with a CCD imager. Then, thin gold metal layers of different thicknesses were sputtered onto the dielectric-grating surface. After a 50 nm gold layer was deposited, the optical resonance could not be revealed from the zero-order transmission. However, the optical resonance can still be obtained from the first-order diffraction by using a CCD. Finally, we deposited a thin BSA protein layer onto the surface of the device. A large optical resonance shift was observed in the first-order diffraction spectrum, while no optical resonance was found in the zero-order transmission. The demonstrated biochemical sensor technique eliminates the need to use a traditional optical spectrometer for resonance spectral measurement, which can reduce the size and cost of the biochemical sensors. The work in this Letter shows that there are significant advantages to measuring optical resonance in the first-order diffraction rather than going the traditional route of measuring the optical resonance in the transmission or reflection for biochemical sensor applications.

This work was partially supported by the United States Department of Agriculture (USDA) National Institute of Food and Agriculture through the Award No. 2014-67022-21618. It was also partially supported by the National Science Foundation (NSF) through grant NSF-1158862. Hong Guo acknowledges the support of the Alabama Graduate Research Scholars Program (GRSP).

References

1. S. Wang, R. Magnusson, and J. Bagby, J. Opt. Soc. Am. **7**, 1470 (1990).
2. S. S. Wang and R. Magnusson, Appl. Opt. **32**, 2606 (1993).
3. Z. S. Liu, S. Tibuleac, D. Shin, P. P. Young, and R. Magnusson, Opt. Lett. **23**, 1556 (1998).
4. M. J. Uddin, T. Khaleque, and R. Magnusson, Opt. Express **22**, 12307 (2014).
5. Y. Ding and R. Magnusson, Opt. Express **12**, 5661 (2004).
6. R. Magnusson, J. Biosens. Bioelectron. **04**, 1 (2013).
7. T. W. Ebbesen, H. J. Lezec, H. F. Ghaemi, T. Thio, and P. A. Wolff, Nature **391**, 667 (1998).
8. L. Martín-Moreno, F. J. García-Vidal, H. J. Lezec, K. M. Pellerin, T. Thio, J. B. Pendry, and T. W. Ebbesen, Phys. Rev. Lett. **86**, 1114 (2001).
9. S.-H. Chang, S. Gray, and G. Schatz, Opt. Express **13**, 3150 (2005).
10. H. Lezec and T. Thio, Opt. Express **12**, 3629 (2004).
11. H. Liu and P. Lalanne, J. Opt. A Pure Appl. Opt. **27**, 2542 (2010).
12. A. Y. Nikitin, F. J. García-Vidal, and L. Martín-Moreno, Phys. Rev. Lett. **105**, 073902 (2010).
13. H. Leong and J. Guo, Opt. Lett. **36**, 4764 (2011).
14. J. Guo and H. Leong, Appl. Phys. Lett. **101**, 241115 (2012).
15. J. Guo and H. Leong, J. Opt. Soc. Am. B **29**, 1 (2012).
16. H. Leong and J. Guo, Opt. Express **20**, 21318 (2012).
17. J. Homola, S. Yee, and G. Gauglitz, Sens. Actuators B **54**, 3 (1999).
18. J. Homola, Sens. Actuators B **41**, 207 (1997).
19. V. Silin, H. Weetall, and D. Vanderah, J. Colloid Interface Sci. **185**, 94 (1997).
20. H. Arwin, Appl. Spectrosc. **40**, 313 (1986).